Research Article

Yun Ouyang, Md Faisal Md Basir*, Kohilavani Naganthran, and Ioan Pop

Stability analysis of unsteady ternary nanofluid flow past a stretching/shrinking wedge

https://doi.org/10.1515/phys-2025-0148
received October 27, 2024; accepted January 05, 2025

Abstract: Slit die extrusion depends highly on fluid temperature and flow properties, which play a crucial role in determining material quality. This research aims to enhance product quality in extrusion processes by deriving a mathematical model from the extrusion process, ensuring practical relevance to industrial applications. The study focuses on the stability analysis of unsteady ternary nanofluid flow past a stretching/shrinking wedge, incorporating viscous dissipation and Joule heating. A key novelty of this work lies in identifying the critical values for the existence of dual solutions and conducting a comprehensive stability analysis. The findings reveal that the first solution is stable, whereas the second is unstable. Critical values are determined using the boundary value problem solver using 4th-order collocation method function in Matlab, and the effects of key parameters – such as the wedge parameter, Eckert number, suction/injection parameter (S), and hybridity – are analyzed through graphical representations. Results show that for a shrinking wedge, the skin friction coefficient and Nusselt number increase with higher values of the unsteadiness parameter, nanoparticle volume fraction, and S. When $\lambda > -3.23$ (shrinking wedge), the ternary nanofluid demonstrates superior thermal transfer compared to binary and mono nanofluids. This study provides a critical foundation for validating advanced models and optimizing heat transfer performance in industrial processes, paving the way for enhanced applications in extrusion and thermal management systems.

Keywords: ternary nanofluid, unsteady flow, wedge flow, viscous dissipation, ohmic heating, stability analysis

*** Corresponding author: Md Faisal Md Basir,** Department of Mathematical Sciences, Faculty of Science, Universiti Teknologi Malaysia, 81310 Johor Bahru, Johor, Malaysia, e-mail: mfaisalmbasir@utm.my
Yun Ouyang: School of Mathematics and Physics, Hechi University, 546300 Yizhou, Guangxi, China; Department of Mathematical Sciences, Faculty of Science, Universiti Teknologi Malaysia, 81310 Johor Bahru, Johor, Malaysia; Key Laboratory of AI and Information Processing, Education Department of Guangxi Zhuang Autonomous Region, Hechi University, 546300 Yizhou, Guangxi, China
Kohilavani Naganthran: Institute of Mathematical Sciences, Faculty of Science, Universiti Malaya, 50603 Kuala Lumpur, Malaysia; Center for Data Analytics, Consultancy and Services, Faculty of Science, Universiti Malaya, 50603 Kuala Lumpur, Malaysia, e-mail: kohi@um.edu.my
Ioan Pop: Department of Mathematics, Babes-Bolyai University, R-400084, Cluj-Napoca, Romania
ORCID: Yun Ouyang 0000-0003-3226-1451; Md Faisal Md Basir 0000-0001-5199-2693; Kohilavani Naganthran 0000-0001-8683-0774; Ioan Pop 0000-0002-0660-6543

Nomenclature

HNF	binary hybrid nanofluid
NF	mono hybrid nanofluid
THNF	ternary hybrid nanofluid
ODEs	ordinary differential equations
PDEs	partial differential equations
BVPs	boundary value problems
Roman letters	
A	unsteadiness parameter
a	positive constant
c	non-negative constant
C_f	skin friction coefficient
C_p	specific heat capacity (J kg^{-1} K^{-1})
k	thermal conductivity (W mK^{-1})
l	characteristic length (m)
m	wedge angle parameter
Nu_x	Nusselt number
Pr	Prandtl number
Re_x	Reynolds number
S	suction/injection parameter
T	temperature (K)
T_∞	temperature far away from the sheet (K)
u, v	velocity component in the x and y directions (m s^{-1})
U_w	stretching surface velocity (m s^{-1})
v_w	mass flux velocity (m s^{-1})
u_e	ambient velocity (m s^{-1})
ρC_p	heat capacitance (J m^{-3} K^{-1})

Greek symbols

β	dimensionless wedge gradient parameter
η	dimensionless similarity variable
λ	stretching/shrinking parameter
μ	dynamic viscosity (N s m^{-2})
ν	kinematic viscosity (m^2 s^{-1})
ϕ_1	cupric nanoparticle volume fraction
ϕ_2	magnesia nanoparticle volume fraction
ϕ_3	titania nanoparticle volume fraction
ρ	density (kg m^{-3})
θ	dimensionless temperature

Subscripts

f	fluid
hnf	hybrid nanofluid
nf	nanofluid
thnf	ternary hybrid nanofluid
1	cupric
2	magnesia
3	titania
w	wall

1 Introduction

Slit die extrusion requires precise control of the fluid's thermal and flow properties to achieve optimal product characteristics and enhance processing efficiency. In this context, the addition of ternary hybrid nanofluids, which comprise three types of nanoparticles dispersed in a base fluid, plays a crucial role. Nanoparticles improve the fluid's thermal conductivity and viscosity, enabling better heat transfer and flow behavior during the extrusion process. For instance, Said *et al.* [1] studied ternary nanofluids composed of rGO-Fe_3O_4-TiO_2 hybrid nanocomposites in ethylene glycol to determine the optimal nanofluid composition for maximizing heat transfer. Their findings, supported by machine learning analysis, revealed that higher nanoparticle concentrations significantly enhance heat transfer performance by modifying viscosity and density under varying conditions. Slit die extrusion also benefits from identifying ideal nanoparticle combinations and stability to improve processing outcomes. Mousavi *et al.* [2] investigated *C*-type nanofluids with a mass ratio of 6:3:1 (CuO:MgO:TiO_2) and 2:1:1 volume fraction. Their study showed that CuO-MgO-TiO_2/water-based nanofluids exhibit excellent thermal conductivity, making them suitable for enhancing heat transfer in extrusion processes. Such findings underscore the potential of carefully designed nanofluids for achieving superior thermal and flow performance during slit die extrusion.

Slit die extrusion processes are deeply connected to foundational fluid dynamics concepts, such as boundary layer theory. Introduced by Prandtl [3] in 1904, this theory provides the framework for understanding the distinction between steady and unsteady flows. Unsteady flows, characterized by temporal variations in velocity and pressure, have applications across multiple industries. Pop *et al.* [4] reviewed the significance of unsteady boundary layer flows in fields like aerospace, turbine engineering, and nanofluid applications. Their work highlights how nanofluids enhance thermal conductivity in permeable materials and microparticle fluids, transforming governing equations into ordinary differential equations (ODEs) to analyze mass transfer, micropolar effects, and flow dynamics. Ouyang *et al.* [5] investigated an Al_2O_3-Cu/water nanofluid mixture to improve water cleanliness by enhancing thermal transfer and facilitating material breakdown. Their study, focusing on flow dynamics in stagnation regions within permeable media, demonstrates the potential of unsteady hybrid nanofluid flows in optimizing water systems and addressing environmental challenges.

In 1931, Falkneb and Skan [6] expanded on Prandtl's boundary layer theory by developing wedge flow theory, describing fluid flow in directions not parallel to the primary flow. This theory has been extensively applied in various fields. Notably, Seddeek *et al.* [7] investigated steady Falkner–Skan (F-S) flow and thermal transfer over a wedge with variable viscosity and heat conductivity, significantly advancing the understanding of such flows. The F-S boundary layer flow equation, which addresses boundary layer flow with a streamwise pressure gradient, has been widely studied. For example, Fang and Zhang [8] and Weidman *et al.* [9] independently conducted numerical analyses of the F-S equation cases. Abbasbandy and Hayat [10] also explored different aspects of these solutions, contributing valuable insights into fluid flow behavior. Zhang *et al.* [11] examined the flow and thermal characteristics of a radiating homogeneous hybrid nanofluid over a stationary wedge surface, highlighting the effects of heat buoyancy forces, Lorentz forces, and Darcy forces on the cooling performance of the hybrid nanofluid. Riley and Weidman [12] analyzed pressure-driven flow over a stretching boundary, revealing multiple solution possibilities and the existence of similar solutions. Ishak *et al.* [13] studied the boundary layer flow of a conductive fluid perpendicular to a changing magnetic field along a moving wedge, providing insights into complex flow conditions.

Joule heating, a mechanism for converting electrical energy into thermal energy, involves heat generation through a decay layer. Research by Shagaiya Daniel

examined radiation and ohmic heating effects on nanofluids. Teh and Ashgar [14] studied 3D mixed nanofluid flow across a rotationally deformable surface under ohmic heating, finding that increasing magnetic parameters increased the velocity but decreased the temperature. Yan *et al.* [15] analyzed Joule heating effects on mixed nanoparticle fluid flow over an exponential surface, noting that $\mathrm{Re}_x^{1/2;}Cf$ increased with magnetic and suction parameters while decreasing with velocity slip factor. They also found that temperature in the dual solution increased with Eckert number, but boundary layer separation remained unaffected. This was consistent with Khashi'ie *et al.* [16], who observed that the Eckert number did not influence the separation point. According to Kishore *et al.* [17], thermal dissipation in natural convective flow, characterized by the Eckert number, is crucial in both natural and industrial processes. High-viscosity fluid flow along elongated structures involves significant viscous and ohmic dissipations, essential for heat transfer. Zeeshan *et al.* [18] investigated Ohmic heating and viscous dissipation in magnetic nanofluids over a sinusoidal wavy surface. Zainal *et al.* [19] explored viscous dissipation and hybrid nanofluid flow over a surface undergoing exponential stretching or shrinking, finding that viscous dissipation increased the thermal state, enlarging the temperature boundary layer. Ouyang *et al.* [20] researched time-dependent MHD ternary nanofluid flow over a moving wedge, developing a comprehensive model that included viscous dissipation and Joule heating. Their findings highlighted enhanced heat transfer and improved surface finish, applicable to industrial processes like slit die extrusion. This study extends the understanding of MHD effects in nanofluid dynamics and provides a theoretical basis for optimizing manufacturing techniques involving complex fluid behaviors.

Stability analysis is used to determine the response of the solution to perturbations. Stable solutions can be used in actual production. Stability analysis can help inform our understanding of the physical properties of different solutions. Merkin [21] applied stability analysis framework to his earlier work [22] on boundary layer and mixed repulsion flow against an upright plane in a fully permeated porous environment. These insights set a precedent, leading many researchers to adopt Merkin's stability analysis and results in their examination of dual solutions' stability. Subsequent studies, such as those by Bachok *et al.* [23], Harris *et al.* [24], Roşca and Pop [25,26], Najib *et al.* [27], and Yasin *et al.* [28], have followed Merkin's [21] analytical approach to determine the stability of solutions in their respective investigations. This framework has since been extended to encompass the stability analysis of two solutions in nanofluid flow (including NF, HNF, and THNF), marking a significant evolution in the study of fluid dynamics within boundary layers.

Slit die extrusion requires precise control of fluid thermal and flow properties, making it essential to incorporate nanoparticles for enhancing thermal conductivity and viscosity. The current study explores the stability analysis of unsteady ternary nanofluid flow over a stretching/shrinking wedge, incorporating viscous dissipation and Joule heating – an area that has been insufficiently addressed in prior research. A key novelty of this study lies in identifying the critical values for the existence of dual solutions and conducting a comprehensive stability analysis. By understanding these critical values, the study provides insights into predicting temperature distributions and maintaining thermal stability, which are vital for ensuring product quality in extrusion processes. Optimizing these factors enables manufacturers to achieve greater uniformity, reduce defects, and enhance efficiency in sectors such as polymers, food processing, and composite materials. This research not only addresses a significant gap in the literature but also lays a robust foundation for validating advanced models and optimizing heat transfer processes in industrial applications. This research aims to improve thermal efficiency in slit die extrusion and addresses the following key questions:

- Which solution is stable?
- How do viscous dissipation and Joule heating impact heat transfer?
- How do factors like fluid type, unsteadiness parameter (A), nanoparticle volume fraction (ϕ), suction/injection parameter (S), and wedge angle (β) affect fluid dynamics and heat transfer?

2 Mathematical formulation

Consider dual solutions of the unsteady boundary layer nanofluid flow over a moving wedge with viscous dissipation and Joule heating, as shown in Figure 1, where the flow being at $y \geq 0$. The velocity of the stretching/shrinking wedge is $U_\mathrm{w}(x,t) = u_\mathrm{w}(x,t)\lambda$, where $u_\mathrm{w}(x,t) = U_0 x^m/(1-ct)$, and that of the far-field inviscous flow is $U_e(x,t) = U_0 x^m/(1-ct)$, where U_0, U_∞, and m are constants, $0 \leq m \leq 1$, $\lambda = U_\infty/U_0$, $\lambda < 0$ stands for the shrinking wedge, $\lambda = 0$ for a steady wedge, $\lambda > 0$ for stretching, respectively. The variable mass flux velocity is $v = v_\mathrm{w}(x,t)$ with $v_\mathrm{w}(x,t) > 0$ for suction and $v_\mathrm{w}(x,t) < 0$ for injection. The variable surface temperature at the surface of the wedge is $T_\mathrm{w}(x,t) = T_\infty + T_0(x/l)^{2m}/(1-ct)^2$, where T_0 is the temperature characteristic of the surface of the wedge, l is the length characteristic of the wedge, and T_∞ represents the free stream temperature. The fluid is CuO-MgO-TiO_2/water. In the context of this study, it is also assumed that the thermal equilibrium is maintained between the water

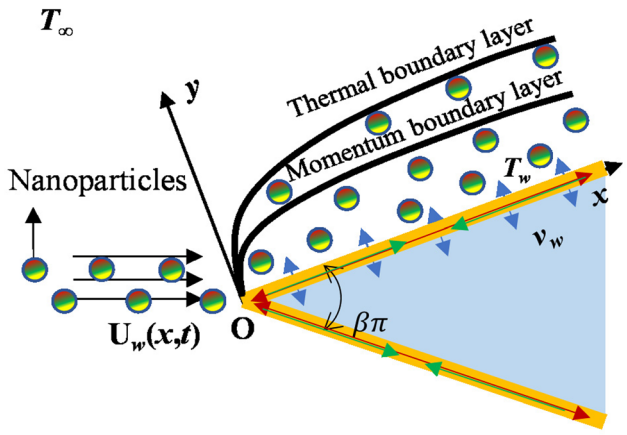

Figure 1: The physical model and coordinate system.

and the dispersed nanoparticles. Moreover, it is presumed that the nanoparticles exhibit uniform characteristics in terms of both size and shape, and that they are in a state of thermal equilibrium.

Using the above statements and assumptions, the control equations can be set forth as [29]

$$\frac{\partial u}{\partial x} + \frac{\partial v}{\partial y} = 0, \tag{1}$$

$$\frac{\partial u}{\partial t} + u\frac{\partial u}{\partial x} + v\frac{\partial u}{\partial y} = \frac{\partial u_e}{\partial t} + u_e\frac{\partial u_e}{\partial x} + \frac{\mu_{\text{thnf}}}{\rho_{\text{thnf}}}\frac{\partial^2 u}{\partial y^2}, \tag{2}$$

$$\frac{\partial T}{\partial t} + u\frac{\partial T}{\partial x} + v\frac{\partial T}{\partial y} = \frac{k_{\text{thnf}}}{(\rho C_p)_{\text{thnf}}}\frac{\partial^2 T}{\partial y^2} + \frac{\mu_{\text{thnf}}}{(\rho C_p)_{\text{thnf}}}\left(\frac{\partial u}{\partial y}\right)^2, \tag{3}$$

subject to

$$\begin{aligned}
&\text{At} \quad y = 0\\
&t < 0: \quad u = 0, \quad v = 0, \quad T = T_\infty\\
&t \geq 0: \quad u = U_{\text{w}}(x,t) = \frac{u_{\text{w}}(x)}{1-ct}\lambda = \frac{U_0 x^m}{1-ct}\lambda,\\
&v = v_{\text{w}}(t), \quad T_{\text{w}}(x,t) = T_\infty + \frac{T_0(x/l)^{2m}}{(1-ct)^2}\\
&\text{when} \quad y \to \infty, \quad u = u_e(x,t) \to \frac{U_0 x^m}{1-ct}, \quad T \to T_\infty,
\end{aligned} \tag{4}$$

where (u, v) are the velocity components of the hybrid nanofluid along (x, y)-axis, T is the temperatures of the hybrid nanofluid. The pressure gradient parameter m, which represents the exponent, is determined by the wedge angle parameter. In this case, we consider the total apex angle of the wedge as $\beta\pi$ and denote it as $m = \frac{\beta}{2-\beta}$ or $\beta = \frac{2m}{m+1}$. White and Majdalani [30] defined the wedge parameter as a parameter that is related to the pressure gradient. Non-negative values of the wedge parameter indicate that when $\beta = 0$ $(m = 0)$, it illustrates the boundary layer flow past a parallel flat plate. On the other hand, when $\beta = 1$ $(m = 1)$, it correlates with a vertical plate.

Further, the ternary nanofluid's physical characteristics μ_{thnf}, ρ_{thnf}, k_{thnf}, $(\rho Cp)_{\text{thnf}}$, and σ_{thnf} are described by [4]

$$\begin{aligned}
\frac{\mu_{\text{thnf}}}{\mu_{\text{f}}} &= \frac{1}{(1-\phi_1)^{2.5}(1-\phi_2)^{2.5}(1-\phi_3)^{2.5}}\\
\frac{\rho_{\text{thnf}}}{\rho_{\text{f}}} &= (1-\phi_3)\left\{(1-\phi_2)\left[(1-\phi_1) + \phi_1\frac{\rho_1}{\rho_{\text{f}}}\right] + \phi_2\frac{\rho_2}{\rho_{\text{f}}}\right\}\\
&\quad + \phi_3\frac{\rho_3}{\rho_{\text{f}}}\\
\frac{(\rho Cp)_{\text{thnf}}}{(\rho Cp)_{\text{f}}} &= (1-\phi_3)\left\{(1-\phi_2)\left[(1-\phi_1) + \phi_1\frac{(\rho Cp)_1}{(\rho Cp)_{\text{f}}}\right]\right.\\
&\quad \left. + \phi_2\frac{(\rho Cp)_2}{(\rho Cp)_{\text{f}}}\right\} + \phi_3\frac{(\rho Cp)_3}{(\rho Cp)_{\text{f}}}\\
\frac{k_{\text{thnf}}}{k_{\text{hnf}}} &= \frac{k_3 + 2k_{\text{hnf}} - 2\phi_3(k_{\text{hnf}} - k_3)}{k_3 + 2k_{\text{hnf}} + \phi_3(k_{\text{hnf}} - k_3)},\\
\text{where} \quad \frac{k_{\text{hnf}}}{k_{\text{nf}}} &= \frac{k_2 + 2k_{\text{nf}} - 2\phi_2(k_{\text{nf}} - k_2)}{k_2 + 2k_{\text{nf}} + \phi_2(k_{\text{nf}} - k_2)},\\
\frac{k_{\text{nf}}}{k_{\text{f}}} &= \frac{k_1 + 2k_{\text{f}} - 2\phi_1(k_{\text{f}} - k_1)}{k_1 + 2k_{\text{f}} + \phi_1(k_{\text{f}} - k_1)},
\end{aligned} \tag{5}$$

where ϕ represents the volume fraction of the nanofluid. When ϕ equals 0, it corresponds to a regular fluid, often referred to as a classical viscous fluids. The dynamic viscosity is denoted as μ, densities as ρ, thermal diffusivities as k, heat capacities as ρCp, and electrical conductivities as σ. Additionally, Cp represents the thermal capacity. In Table 1, the physical characteristics of the water and nanoparticles are provided.

To solve Eqs (1)–(3), it is appropriate to present the ensuing similarity transformations

$$\begin{aligned}
u &= \frac{U_{\text{w}}(x)}{1-ct}f'(\eta),\\
v &= -\sqrt{\frac{(m+1)\nu_{\text{f}}U_{\text{w}}(x)}{2x(1-ct)}}\left(f + \frac{m-1}{m+1}\eta f'\right)\\
T(x,t) &= T_\infty + T_0(x/l)^{2m}\theta(\eta)/(1-ct)^2,\\
\eta &= y\sqrt{\frac{(m+1)U_{\text{w}}(x)}{2\nu_{\text{f}}x(1-ct)}},
\end{aligned} \tag{6}$$

and

Table 1: Thermophysical properties (Adnan and Ashraf [31])

Physical characteristics	H_2O	CuO	MgO	TiO_2
ρ (kg m^{-3})	997.1	6,320	3,560	4,250
C_p (J kg^{-1} K)	4,179	531.8	955	686.2
k (W m^{-1} K)	0.613	76.5	45	8.953

$$v_w(x,t) = -\sqrt{\frac{(m+1)\nu_f U_w(x)}{2x(1-ct)}}\,S. \tag{7}$$

In this passage, the symbol prime represents differentiation with respect to variable η. The symbol S represents the constant mass flux velocity, with a positive value of S indicating suction of the fluid, and a negative value indicating injection of the fluid.

By substituting Eq. (6) in Eqs (2)–(4), we can derive the subsequent equations for similarity.

$$\frac{\mu_{thnf}/\mu_f}{\rho_{thnf}/\rho_f} f''' + ff'' + \beta(1-f'^2) - A\left(f' + \frac{\eta}{2}f'' - 1\right) = 0 \tag{8}$$

$$\frac{1}{\Pr}\frac{k_{thnf}/k_f}{(\rho C_p)_{thnf}/(\rho C_p)_f}\theta'' + f\theta' - 2\beta f'\theta - A\left(2\theta + \frac{\eta\theta'}{2}\right) + \frac{\mathrm{Ec}}{(\rho C_p)_{thnf}/(\rho C_p)_f}\left(\frac{\mu_{thnf}}{\mu_f}(f'')^2\right) = 0 \tag{9}$$

along with

$$\begin{aligned} &f(0) = S, \quad f'(0) = \lambda, \quad \theta(0) = 1 \\ &f'(\eta) \to 1, \quad \theta(\eta) \to 0 \quad \text{as } \eta \to \infty, \end{aligned} \tag{10}$$

where Pr is the Prandtl number, A is the unsteadiness parameter, β is the wedge parameter, and Ec is the Eckert number, described as

$$\begin{aligned} &\Pr = \frac{(\mu C_p)_f}{k_f}, A = \frac{2xc}{(m+1)U_0 x^m}, \beta = \frac{2m}{m+1}, \\ &\mathrm{Ec} = \frac{u_w(x,t)^2}{(Cp)_f(T_w - T_\infty)} = \frac{U_0^2 x^{2m}/(1-ct)^2}{T_0(x/l)^{2m}(Cp)_f/(1-ct)^2} \\ &\quad = \frac{U_0^2 l^{2m}}{T_0(Cp)_f}, \end{aligned} \tag{11}$$

where C_f and Nu_x are characterized as

$$\begin{aligned} C_f &= \frac{\mu_{thnf}}{\rho_f u_e^2(x,t)}\left(\frac{\partial u}{\partial y}\right)_{y=0}, \\ \mathrm{Nu}_x &= -\frac{x k_{thnf}}{k_f[T_w(x) - T_\infty]}\left(\frac{\partial T}{\partial y}\right)_{y=0}. \end{aligned} \tag{12}$$

Using Eqs (6) and (12), we obtain

$$\begin{aligned} \mathrm{Re}_x^{1/2} C_f &= \frac{\mu_{thnf}}{\mu_f}\sqrt{\frac{m+1}{2}}f''(0), \\ \mathrm{Re}_x^{-1/2}\mathrm{Nu}_x &= -\frac{k_{thnf}}{k_f}\sqrt{\frac{m+1}{2}}\theta'(0), \end{aligned} \tag{13}$$

where $\mathrm{Re}_x = u_w(x)x/\nu_f$ is the local Reynolds number.

3 Stability analysis

The stability of the non-unique solutions provided by Eqs (8)–(10) is evaluated in this section. $\tau = \frac{c}{A}\frac{t}{(1-ct)}$ is introduced.

$$\begin{aligned} &u(x,y,t,\tau) = \frac{U_0 x}{1-ct}\frac{\partial f}{\partial \eta}(\eta,\tau), \\ &v = v_w(t,\tau) = -\sqrt{\frac{a\nu_f}{1-ct}}f(\eta,\tau), \quad \theta(\eta,\tau) = \frac{T - T_\infty}{T_w - T_\infty}, \\ &\eta = y\sqrt{\frac{a}{\nu_f(1-ct)}}, \quad \tau = \frac{c}{A}\frac{t}{(1-ct)}. \end{aligned} \tag{14}$$

Thus,

$$\frac{\mu_{thnf}/\mu_f}{\rho_{thnf}/\rho_f} f_{\eta\eta\eta} + ff_{\eta\eta} + \beta(1-f_\eta^2) - A\left(f_\eta + \frac{\eta}{2}f_{\eta\eta} - 1\right) - (1+A\tau)f_{\eta\tau} - \tau\frac{2(m-1)}{m+1}f_\eta f_{\eta\tau} = 0, \tag{15}$$

$$\frac{1}{\Pr}\frac{k_{thnf}/k_f}{(\rho C_p)_{thnf}/(\rho C_p)_f}\theta_{\eta\eta} + \frac{\mathrm{Ec}}{(\rho C_p)_{thnf}/(\rho C_p)_f}\left(\frac{\mu_{thnf}}{\mu_f}(f_{\eta\eta})^2\right) + f\theta_\eta - 2\beta f_\eta\theta - A\left(2\theta + \frac{\eta\theta_\eta}{2}\right) - \theta_\tau - \tau\frac{2(m-1)}{m+1}f_\eta\theta_\tau = 0 \tag{16}$$

together with

$$\begin{aligned} &f(0,\tau) = S, \quad \frac{\partial f}{\partial \eta}(0,\tau) = \lambda, \quad \theta(0,\tau) = 1, \\ &\lim_{\eta\to\infty}\frac{\partial f}{\partial \eta}(\eta,\tau) = 0, \quad \lim_{\eta\to\infty}\theta(\eta,\tau) = 0. \end{aligned} \tag{17}$$

The robustness of the similarity solutions $f(\eta) = f_0(\eta)$ and $\theta(\eta) = \theta_0(\eta)$ is examined by employing the following perturbation equation:

$$\begin{aligned} f(\eta,\tau) &= f_0(\eta) + e^{-\varepsilon\tau}F(\eta,\tau), \\ \theta(\eta,\tau) &= \frac{T - T_\infty}{T_f - T_\infty} = \theta_0(\eta) + e^{-\varepsilon\tau}G(\eta,\tau), \end{aligned} \tag{18}$$

where ε is an unknown eigenvalue, $F(\eta,\tau)$ and $G(\eta,\tau)$ are relatively small than $f_0(\eta)$ and $\theta_0(\eta)$. By substituting Eq. (18) in Eqs (15)–(17), the following equations are obtained:

$$\frac{\mu_{thnf}/\mu_f}{\rho_{thnf}/\rho_f}F_{\eta\eta\eta} + f_0F_{\eta\eta} + f''_0F - 2\beta f'_0F_\eta - A\left(F_\eta + \frac{\eta}{2}F_{\eta\eta}\right) + (1+A\tau)(\varepsilon F_\eta - F_{\eta\tau}) - \tau\frac{2(m-1)}{m+1}(f'_0F_{\eta\tau} - \varepsilon f'_0F_\eta) = 0 \tag{19}$$

$$\frac{1}{\Pr}\frac{k_{\text{thnf}}/k_{\text{f}}}{(\rho C_p)_{\text{thnf}}/(\rho C_p)_{\text{f}}}G_{\eta\eta} + \frac{2\text{Ec}}{(\rho C_p)_{\text{thnf}}/(\rho C_p)_{\text{f}}} \times \left(\frac{\mu_{\text{thnf}}}{\mu_{\text{f}}}f''_0 F_{\eta\eta}\right) + f_0 G_\eta + F\theta'_0 - A\left(2G + \frac{\eta G_\eta}{2}\right) - 2\beta(f'_0 G + F_\eta\theta_0) + (1 + A\tau)(\varepsilon G - G_\tau) - \tau\frac{2(m-1)}{m+1}(f'_0 G_\tau - \varepsilon f'_0 G) = 0 \quad (20)$$

together with

$$F(0,\tau) = 0, \quad F_\eta(0,\tau) = 0, \quad G(0,\tau) = 0, \quad \lim_{\eta\to\infty} F_\eta(\eta,\tau) \to 0, \quad \lim_{\eta\to\infty} G(\eta,\tau) \to 0. \quad (21)$$

Let $\tau = 0$.

$$\frac{\mu_{\text{thnf}}/\mu_{\text{f}}}{\rho_{\text{thnf}}/\rho_{\text{f}}}F_0''' + f_0 F''_0 + f''_0 F_0 - 2\beta f'_0 F'_0 - A\left(F'_0 + \frac{\eta}{2}F''_0\right) + \varepsilon F'_0 = 0 \quad (22)$$

$$\frac{1}{\Pr}\frac{k_{\text{thnf}}/k_{\text{f}}}{(\rho C_p)_{\text{thnf}}/(\rho C_p)_{\text{f}}}G''_0 + \frac{2\text{Ec}}{(\rho C_p)_{\text{thnf}}/(\rho C_p)_{\text{f}}}\frac{\mu_{\text{thnf}}}{\mu_{\text{f}}}f''_0 F''_0 + f_0 G'_0 + F_0\theta'_0 - 2\beta(f'_0 G_0 + F'_0\theta_0) - A\left(2G_0 + \frac{\eta G'_0}{2}\right) + \varepsilon G_0 = 0 \quad (23)$$

with

$$F_0(0) = 0, \quad F_0'(0) = 0, \quad G_0(0) = 0, \quad F_0'(\eta) = 0, \quad G_0(\eta) = 0, \quad \text{as } \eta \to \infty. \quad (24)$$

Following Harris *et al.* [24], $F'_0(\infty) \to 0$ is eased into $F''_0(0) = 1$.

4 Results and discussion

The boundary value problem solver using 4th-order collocation (BVP4C) method function in MATLAB is developed to solve non-linear boundary value problems. This function is established on the three-stage Lobatto IIIa formula. The core idea behind this method is to transform BVPs into a set of ODEs, as shown in Eqs (8)–(10). Solutions to these problems are illustrated in Figures 2–7. The substantial agreement highlighted in Table 2 bolsters the confidence in the accuracy of our numerical outcomes, thereby reinforcing the credibility of the results.

Figures 2–7 demonstrate the effects of fluid flow on the skin friction coefficient and the Nusselt number. The results indicate the presence of two solutions when $\lambda_{ci} \le \lambda$. However, for $\lambda \le \lambda_{ci} \le 0$ (i = 1, 2, ..., 5), Eqs (8)–(10) lack any solutions. Consequently, Eqs (1)–(4) must be solved using numerical techniques. The critical points $\lambda_{ci} < 0$ (i = 1, 2, 3, 4) indicate the conditions under which real solutions to Eqs (8)–(10) can be found. Stability analysis has shown that the first solution is physically realizable, whereas the second solution is not applicable in practice.

Figure 2 illustrates the enhancement of the Nusselt number but a decrease in the skin friction coefficient as the fluid transitions from NF to HNF to THNF. According to Myers *et al.* [34], the sum of the volume fractions ϕ_1, ϕ_2, and ϕ_3 should be less than 0.05. For this analysis, we assume $\phi_1 + \phi_2 + \phi_3 = 0.04$. The three nanofluid flows considered are: NF with $\phi_1 = 0.04$, $\phi_2 = \phi_3 = 0$; HNF with $\phi_1 = 0.03$, $\phi_2 = 0.01$, $\phi_3 = 0$; and THNF with $\phi_1 = 0.02$, $\phi_2 = \phi_3 = 0.01$ as per Mousavi *et al.* [2].

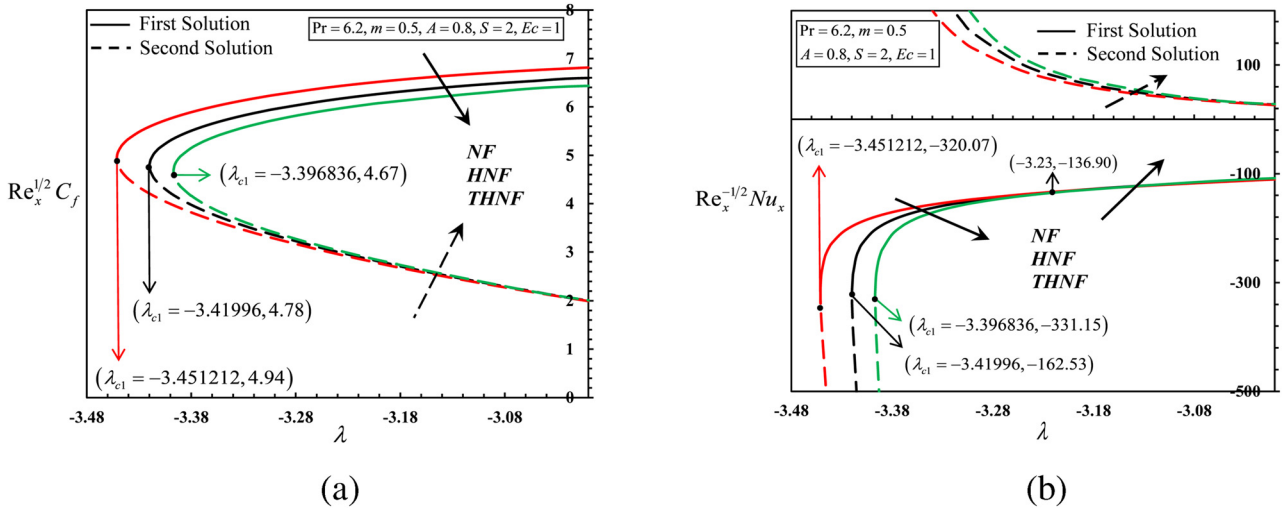

Figure 2: Physical properties for NF, HNF, THNF fluid flow: (a) $\text{Re}_x^{1/2}C_\text{f}$ and (b) $\text{Re}_x^{-1/2}\text{Nu}_x$.

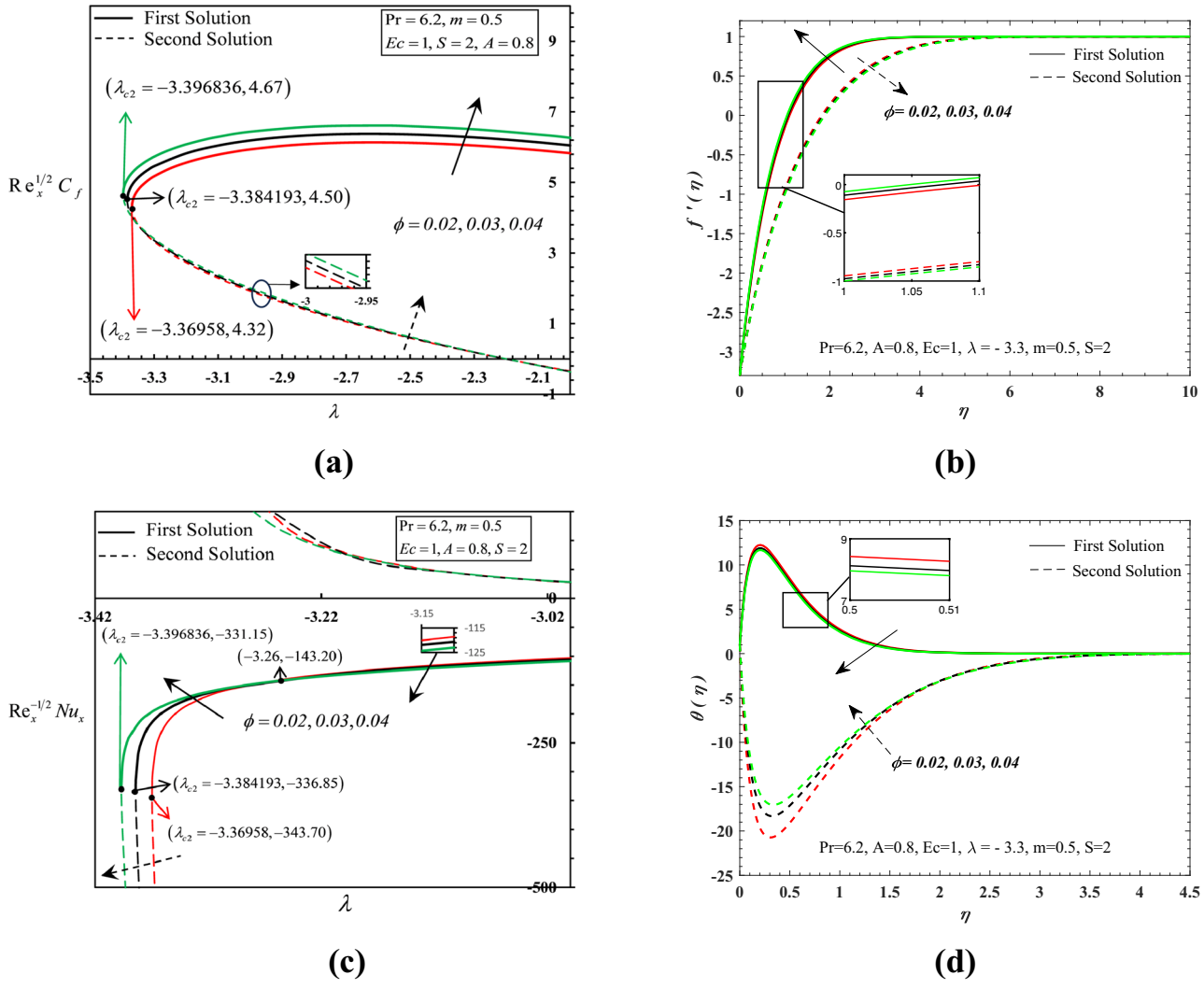

Figure 3: Physical properties for different ϕ values: (a) $\mathrm{Re}_x^{1/2}C_f$, (b) $f'(\eta)$, (c) $\mathrm{Re}_x^{-1/2}\mathrm{Nu}_x$, and (d) $\theta(\eta)$.

The expression of the skin friction coefficient, representing a specific fluid dynamic characteristic, shows a decreasing trend from NF to HNF to THNF. This reduction likely reflects changes in the fluid's viscosity, thermal conductivity, or both, which impact the friction factor at the fluid's surface. In Figure 2(b), the Nusselt number increases as the fluid transitions from NF to HNF to THNF as $\lambda > -3.23$. This aligns with the concept that optimizing nanoparticle concentration can increase the convection mechanism, because surface temperature decreases with rising hybridity. The critical values for NF, HNF, and THNF are −3.451212, −3.41996, and −3.396836, respectively. This progression in critical values indicates accelerated boundary layer separation, suggesting changes in flow characteristics that could differently influence performance in various applications using these fluids.

Figure 3 illustrates the effect of nanoparticle volume fraction (ϕ) on various parameters, including the skin friction coefficient, velocity, the Nusselt number, and temperature profile. As ϕ increases, both the skin friction coefficient and velocity increase, while T decreases. The observed increase in the skin friction coefficient and velocity with rising ϕ can be attributed to the enhanced thermal conductivity and viscosity of the nanofluid, which improve momentum transfer and result in a more robust flow profile. The decrease in temperature (T) is due to the improved heat transfer capabilities of the nanofluid, which facilitates more efficient cooling. For the Nusselt number, the behavior varies depending on the value of λ. When $\lambda < -3.26$, the increased nanoparticle volume fraction enhances the convective heat transfer, leading to a rise in the Nusselt number (Nu_x). Conversely, for $\lambda > -3.26$, the adverse pressure gradient may overpower the

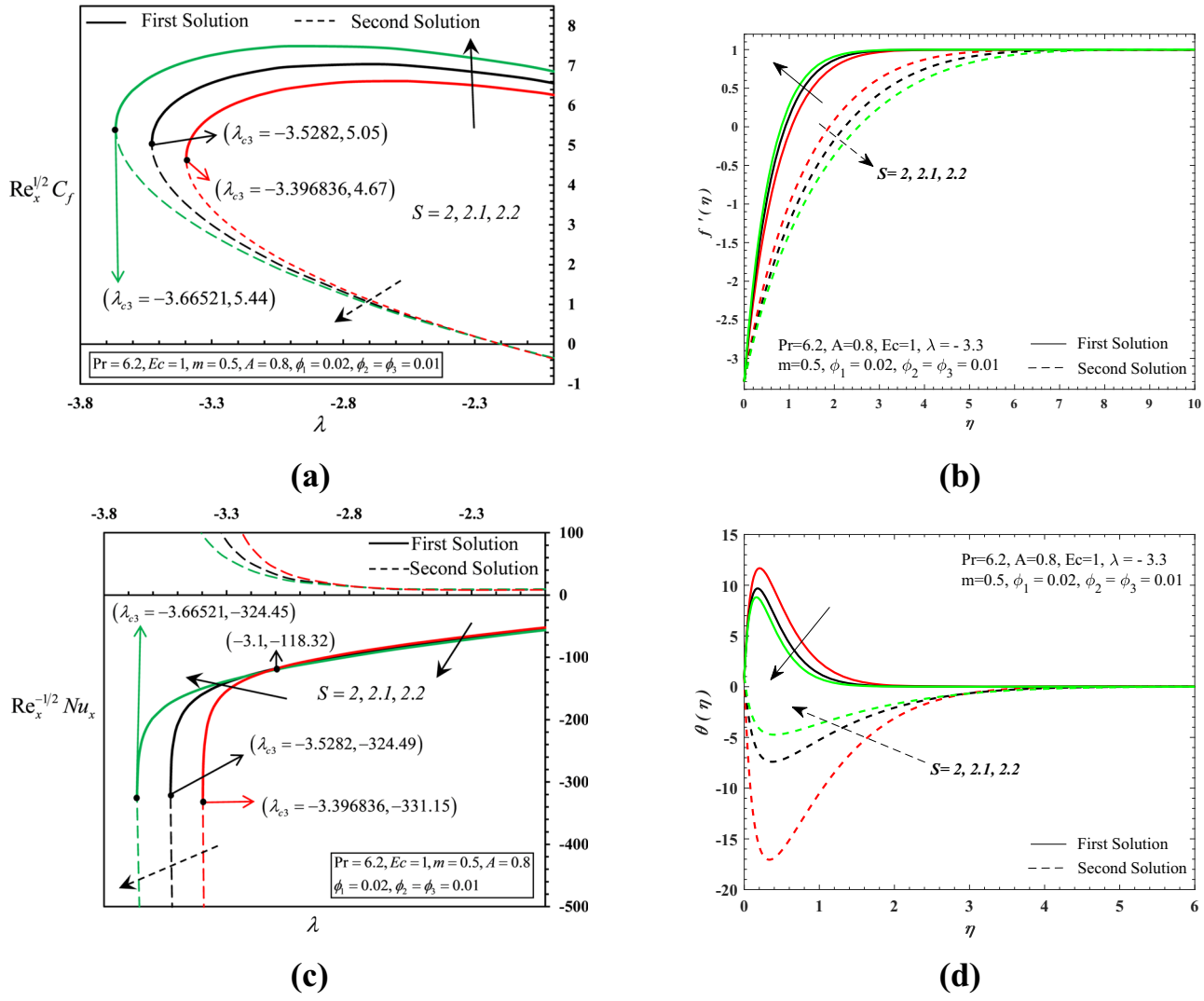

Figure 4: Physical properties for different S values: (a) $\mathrm{Re}_x^{1/2} C_f$, (b) $f'(\eta)$, (c) $\mathrm{Re}_x^{-1/2} \mathrm{Nu}_x$, and (d) $\theta(\eta)$.

beneficial effects of enhanced thermal conductivity, resulting in a reduction in Nu_x.

Additionally, the Nusselt number shows an increase for $\lambda < -3.26$ and a decrease for $\lambda > -3.26$. The increase in ϕ causes the flow separation point to delay, shifting from −3.36958 to −3.384193, and finally to −3.396836. The delay in flow separation with increasing ϕ can be explained by the improved stability of the boundary layer ascribable to the increasing viscosity and thermal conductivity of the nanofluid. These properties contribute to a more stable flow regime, allowing the fluid to adhere to the surface for a longer distance before separating. This delay in flow separation leads to improved aerodynamic performance and reduced drag, which is beneficial in various engineering applications.

Figure 4(a) illustrates the behavior of the skin friction coefficient in the upper branch solution as the wedge experiences shrinkage and S increases. Rising S effect enhances the velocity gradient, resulting in drop in the momentum boundary layer thickness (refer to Figure 4(b)). Conversely, in the lower branch solution, the skin friction coefficient decreases with increasing S. This suggests that the left-moving wedge cannot accommodate further fluid penetration, resulting in a drop in the velocity gradient and a thicker momentum boundary layer, as shown in Figure 4(b).

Both figures indicate that higher S values reduce the boundary layer thickness, as suction diminishes drag force and prevents boundary layer separation. As to temperature, the first solution shows a declining trend with S,

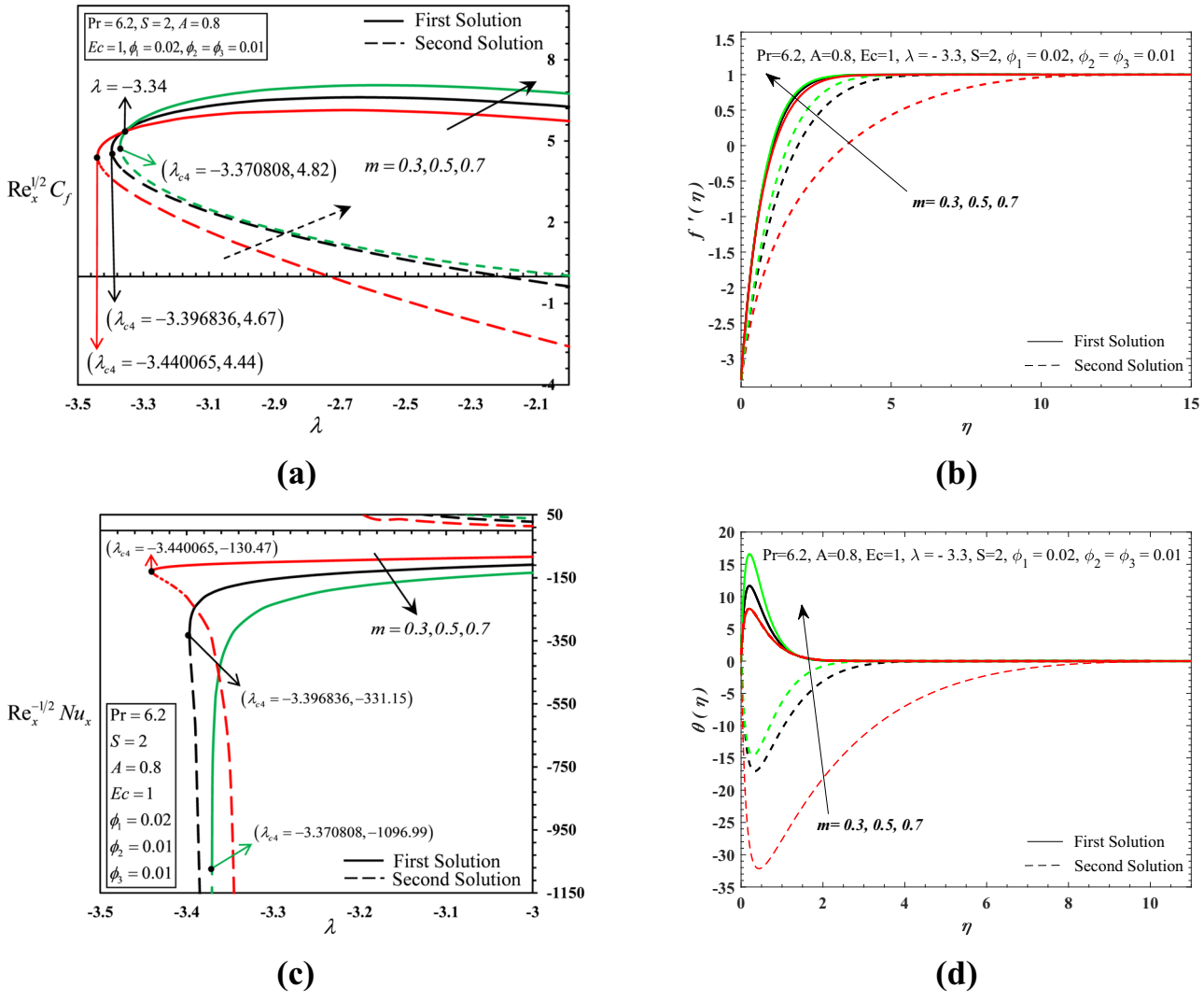

Figure 5: Physical properties for different m values: (a) $\mathrm{Re}_x^{1/2}C_\mathrm{f}$, (b) $f'(\eta)$, (c) $\mathrm{Re}_x^{-1/2}\mathrm{Nu}_x$, and (d) $\theta(\eta)$.

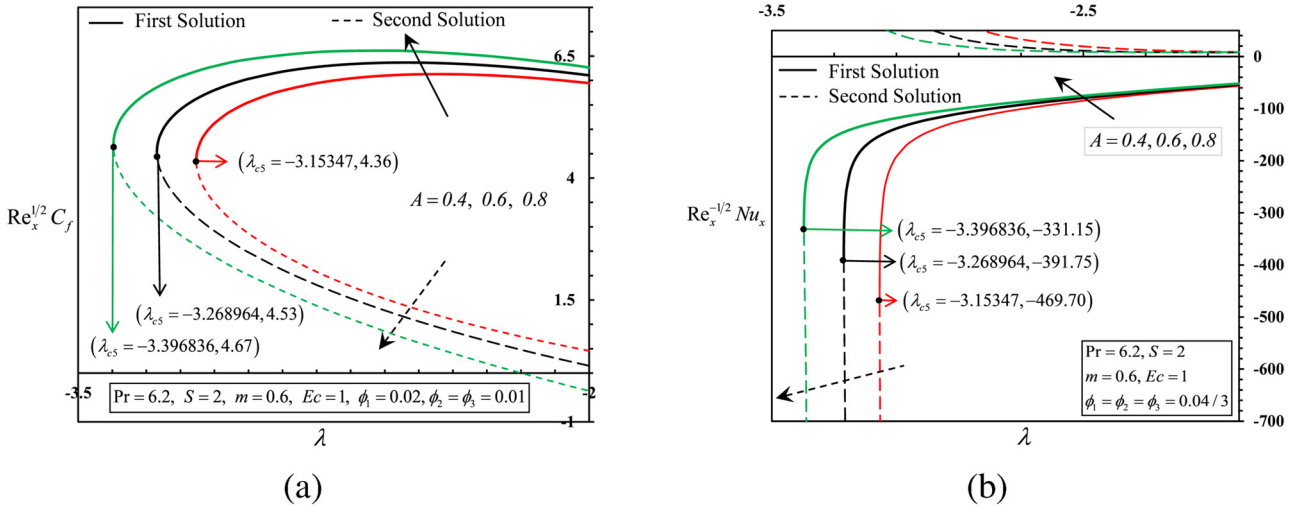

Figure 6: Physical properties for different A values: (a) $\mathrm{Re}_x^{1/2}C_\mathrm{f}$ and (b) $\mathrm{Re}_x^{-1/2}\mathrm{Nu}_x$.

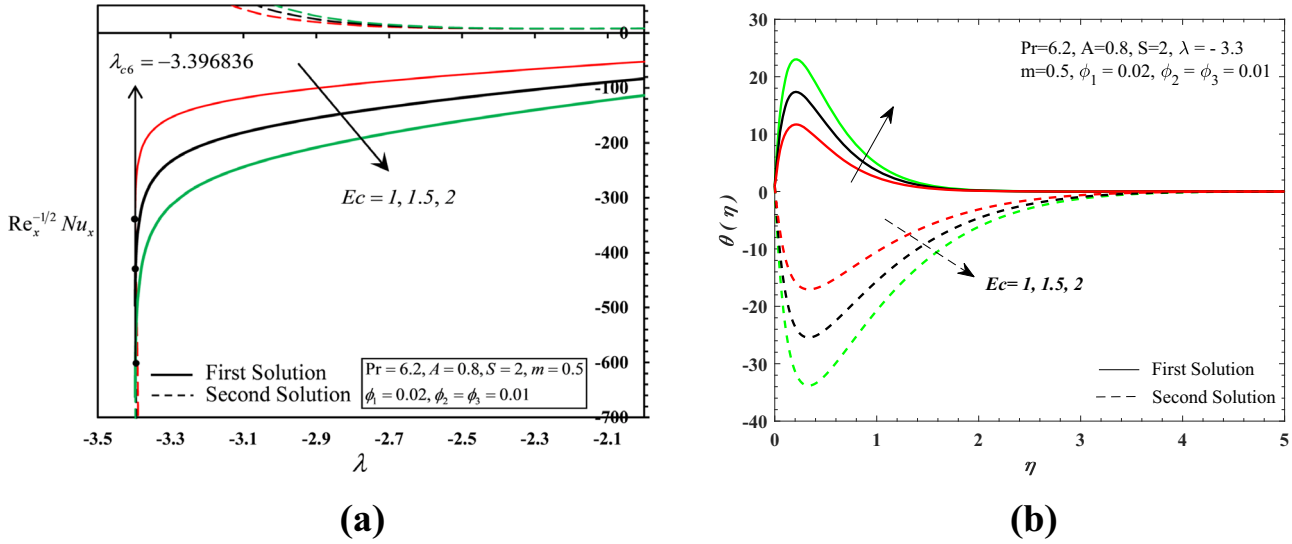

Figure 7: Physical properties for different Ec values: (a) $\mathrm{Re}_x^{-1/2}\mathrm{Nu}_x$ and (b) $\theta(\eta)$.

while the second solution exhibits an escalating trend (refer to Figure 4(d)). This behavior is consistent with the temperature variations depicted in Figure 4(c). The reduction in temperature decreases the thermal diffusivity of the tri-hybrid nanofluid, gradually improving convective heat transfer. As S increases, boundary layer separation is delayed, with the critical value shifting from −3.396836 to −3.5282 and eventually to −3.66521.

Figure 5 illustrates the impact of m on the skin friction coefficient, the Nusselt number, dimensionless velocity, and temperature. As m increases, β rises, indicating that the angle of the wedge is enlarging. For $\lambda > -3.34$, the skin friction coefficient increases with the increase in m. In Figure 5(b), velocity is an increasing function of m, meaning that as the wedge's angle rises, velocity also increases. This might be due to the increased interactions between the fluid and the surface, which impede fluid motion and create resistance to flow.

When $\lambda_c < \lambda < -3.34$, the rapid stretching of the wedge causes the fluid velocity to drop as m rises, leading to a decline in the skin friction coefficient. The temperature increases with m in Figure 5(d), likely due to the opposition created by m, additional energy is converted into heat. As the fluid faces greater resistance, a portion of its kinetic energy is transformed into thermal energy, leading to a rise in temperature.

The Nusselt number decreases with the increase in m, as demonstrated in Figure 5(c). The Nusselt number, which relates convective to conductive heat transfer, decreases, indicating that convective heat exchange is decreasing compared to conductive thermal transfer. This may be attributed to the lowered fluid velocity and heightened resistance to flow, which hinder convective thermal transfer.

In Figure 6(a), it is observed that as A increases, the skin friction coefficient increases when the wedge is

Table 2: Values of $f''(0)$ for the shrinking wedge (Pr = 0.72; $\phi_1 = \phi_2 = \phi_3 = 0$; $S = 0$; Ec = 0; $A = 0$; $m = 1$)

λ	Wang [32]		Naganthran *et al.* [33]		Present result	
	Upper branch	Lower branch	Upper branch	Lower branch	Upper branch	Lower branch
−0.25	1.40224	—	1.4022407	—	1.4022408	—
−0.5	1.49567	—	1.4956697	—	1.4956698	—
−1.0	1.32882	0	1.3288168	0	1.3288169	0
−1.1	—	—	1.1866805	0.0492290	1.1866803	0.0492289
−1.15	1.08223	0.116702	1.0822311	0.1167020	1.0822312	0.1167021
−1.2	—	—	0.9324733	0.2336496	0.9324735	0.2336497
−1.2465	0.5543	—	0.5842759	0.5542976	0.5842819	0.5542962
−1.24657	—	—	0.5745397	0.5640169	0.5745587	0.5640157

shrinking, whereas it decreases with a stretching wedge. This behavior can be attributed to the boundary layer characteristics influenced by the wedge's motion. When the wedge is shrinking, an increase in A enhances the adverse pressure gradient, thickening the boundary layer and increasing the skin friction coefficient, as shown by the rise in the skin friction coefficient. Conversely, for a stretching wedge, the favorable pressure gradient thins the boundary layer, reducing the skin friction and thus, C_f decreases. These effects are pronounced due to the interaction between the wedge's motion and the local flow dynamics.

Additionally, in Figure 6(b), the increase in the Nusselt number with rising A can be attributed to enhanced thermal boundary layer effects. As the Reynolds number, Re_x, decreases (due to the factor of $\mathrm{Re}_x^{-1/2}$), the impact of viscous forces becomes more significant, leading to a thicker thermal boundary layer. This thicker layer facilitates greater thermal exchange between the surface and the fluid, thus increasing Nu_x, which measures the convective thermal transfer on the surface. These results further show that increasing the intensity of unsteadiness enhances thermal transfer efficiency.

In Figure 7, the influence of Ec on thermal exchange distribution is presented. Ec considers the combined effects of Ohmic heating and the magnetic field. As shown in Figure 7(b), an increased Ec results in a higher temperature, indicating more effective convective thermal transfer and enhanced heat diffusivity, which together promote greater heat dissipation. However, despite these improvements, a higher Eckert number ultimately leads to a decrease in the convective heat exchange rate. This occurs because the increased internal temperature of the fluid reduces the temperature gradient between the fluid and its environment, making heat exchange less efficient. When Ec increases, the critical value and the skin friction coefficient remain unchanged.

Table 3: ε for λ, m, and HNF/THNF when Pr = 6.2, m = 0.5

A	Ec	HNF/THNF	λ	1st solution ε	2nd solution ε
0.6	1	THNF	−3.2689	0.018436	−0.018354
			−3.268	0.07144	−0.070232
			−3.26	0.22129	−0.210064
0.8	1.5	THNF	−3.3968	0.013348	−0.0133016
			−3.396	0.064373	−0.0633063
			−3.39	0.186729	−0.1780104
0.8	1	NF	−3.4512	0.0078496	−0.0078338
			−3.451	0.0325714	−0.0323031
			−3.45	0.0782518	−0.0767201

From Table 3, the first solution is stable because $\varepsilon > 0$, while the other one is unstable.

5 Conclusion

This research focuses on developing a numerical solution for unsteady wedge flow, considering viscous dissipation and Joule heating in a ternary CuO–MgO–TiO_2/H_2O nanofluid. Numerical computations are carried out using the BVP4C function in Matlab to analyze the effects of key parameters, including the wedge parameter, nanoparticle volume fraction, suction/injection parameter, and Eckert number. The findings reveal the existence of nonunique solutions over a broad range of control parameters for the ternary nanofluid. This analysis has direct applications in slit die extrusion, where managing fluid properties such as thermal conductivity and viscosity is essential for achieving uniform heat transfer and enhanced material quality. The key discoveries of this research can be listed:

- The first solution is stable, whereas the second solution is unstable.
- The Nusselt number drops as the Eckert number increases.
- The convective heat transfer enhances from mono to binary to ternary nanofluid when $\lambda > -3.23$.
- The boundary layer separation is delayed with rising unsteadiness parameter, nanoparticle volume fraction, and suction/injection parameter while decelerating with increasing type numbers of nanoparticles and wedge angle.
- When the wedge surface is shrinking, the skin friction coefficient and the Nusselt number increase with the rising unsteadiness parameter, nanoparticle volume fraction, and suction/injection parameter.
- When the wedge surface is shrinking, the skin friction coefficient increases with the rising wedge angle parameter, while the Nusselt number drops.

This research provides valuable insights into the flow behavior of ternary nanofluids, offering practical guidance for optimizing heat transfer and improving efficiency in extrusion processes across industries such as polymer manufacturing, food processing, and composite materials. The findings suggest that increasing parameters such as the unsteadiness parameter, nanoparticle volume fraction, and suction/injection parameter can help meet specific industrial requirements, enabling better control over thermal and flow properties.

However, a limitation of this study is its focus on a specific set of parameters, leaving room for further exploration. Future research could expand the scope by

incorporating additional parameters and introducing new conditions, such as velocity slip (Ouyang *et al.* [35]), heat generation/absorption (Ouyang *et al.* [36]), Casson fluid (Naganthran and Nazar [37]), gyro tactic bio-convection flow (Basir *et al.* [38]), cone (Hanif *et al.* [39]), and Brownian motion (Saleem *et al.* [40]). These additions could further refine the understanding of nanofluid behavior and enhance its applicability in industrial processes.

Acknowledgments: The authors would like to acknowledge the financial support from Universiti Teknologi Malaysia for the funding under UTM fundamental Research (UTMFR) [grant number Q.J130000.3854.21H91], Malaysian Ministry of Higher Education [grant number FRGS/1/2023/STG06/UM/02/14], and Key Laboratory of AI and Information Processing (Hechi University), Education Department of Guangxi Zhuang Autonomous Region, China.

Funding information: The authors would like to acknowledge the financial support from Universiti Teknologi Malaysia for the funding under UTM fundamental Research (UTMFR) [grant number Q.J130000.3854.21H91], Malaysian Ministry of Higher Education [grant number FRGS/1/2023/STG06/UM/02/14], and Key Laboratory of AI and Information Processing (Hechi University), Education Department of Guangxi Zhuang Autonomous Region, China.

Author contributions: Yun Ouyang – resources, methodology, software, and writing; Md Faisal Md Basir – funding acquisition, writing, supervision, and project administration; Kohilavani Naganthran – writing, supervision, visualization, and validation; Ioan Pop – writing, methodology, formal analysis, and validation. All authors have accepted responsibility for the entire content of this manuscript and approved its submission.

Conflict of interest: The authors state no conflict of interest.

Data availability statement: All data generated or analyzed during this study are included in this published article.

References

[1] Said Z, Cakmak NK, Sharma P, Sundar LS, Inayat A, Keklikcioglu O, et al. Synthesis, stability, density, viscosity of ethylene glycol-based ternary hybrid nanofluids: Experimental investigations and model-prediction using modern machine learning techniques. Powder Tech. 2022;400:117190.

[2] Mousavi S, Esmaeilzadeh F, Wang X. Effects of temperature and particles volume concentration on the thermophysical properties and the rheological behavior of $CuO/MgO/TiO_2$ aqueous ternary hybrid nanofluid: Experimental investigation. J Thermal Anal Calorimetry. 2019;137:879–901.

[3] Prandtl L. On the motion of a fluid with very small viscosity. In: Proceedings of the Third International Mathematical Congress; 1904. p. 484–91.

[4] Pop I, Groşan T, Revnic C, Roşca AV. Unsteady flow and heat transfer of nanofluids, hybrid nanofluids, micropolar fluids and porous media: A review. Therm Sci Eng Progress. 2023;46:102248.

[5] Ouyang Y, Basir MFM, Naganthran K, Pop I. Effects of discharge concentration and convective boundary conditions on unsteady hybrid nanofluid flow in a porous medium. Case Stud Therm Eng. 2024;58:104374.

[6] Falkneb V, Skan SW. LXXXV. Solutions of the boundary-layer equations. London Edinburgh Dublin Philos Magazine J Sci. 1931;12(80):865–96.

[7] Seddeek M, Afify A, Al-Hanaya A. Similarity solutions for a steady MHD Falkner-Skan flow and heat transfer over a wedge considering the effects of variable viscosity and thermal conductivity. Appl Appl Math Int J. 2009;4(2):6.

[8] Fang T, Zhang J. An exact analytical solution of the Falkner-Skan equation with mass transfer and wall stretching. Int J Non-Linear Mech. 2008;43(9):1000–6.

[9] Weidman P, Kubitschek D, Davis A. The effect of transpiration on self-similar boundary layer flow over moving surfaces. Int J Eng Sci. 2006;44(11-12):730–7.

[10] Abbasbandy S, Hayat T. Solution of the MHD Falkner-Skan flow by homotopy analysis method. Commun Nonl Sci Numer Simulat. 2009;14(9-10):3591–8.

[11] Zhang K, Shah NA, Alshehri M, Alkarni S, Wakif A, Eldin SM. Water thermal enhancement in a porous medium via a suspension of hybrid nanoparticles: MHD mixed convective Falkneras-Skan flow case study. Case Stud Therm Eng. 2023;47:103062.

[12] Riley N, Weidman P. Multiple solutions of the Falkner-Skan equation for flow past a stretching boundary. SIAM J Appl Math. 1989;49(5):1350–8.

[13] Ishak A, Nazar R, Pop I. MHD boundary-layer flow past a moving wedge. Magnetohydrodynamics. 2009;45(1):103–10.

[14] Teh YY, Ashgar A. Three dimensional MHD hybrid nanofluid Flow with rotating stretching/shrinking sheet and Joule heating. CFD Letters. 2021;13(8):1–19.

[15] Yan L, Dero S, Khan I, Mari IA, Baleanu D, Nisar KS, et al. Dual solutions and stability analysis of magnetized hybrid nanofluid with Joule heating and multiple slip conditions. Processes. 2020;8(3):332.

[16] Khashi'ie NS, Arifin NM, Pop I, Wahid NS. Flow and heat transfer of hybrid nanofluid over a permeable shrinking cylinder with Joule heating: A comparative analysis. Alexandr Eng J. 2020;59(3):1787–98.

[17] Kishore P, Bhanumathi D, Verma VS. The influence of chemical reaction and viscous dissipation on unsteady MHD free convection flow past an exponentially accelerated vertical plate with variable surface conditions. Chem Industry Chem Eng Quarter. 2013;19(2):181–93.

[18] Zeeshan A, Majeed A, Akram MJ, Alzahrani F. Numerical investigation of MHD radiative heat and mass transfer of nanofluid

flow towards a vertical wavy surface with viscous dissipation and Joule heating effects using Keller-box method. Math Comput Simulat. 2021;190:1080–109.
[19] Zainal N, Nazar R, Naganthran K, Pop I. Viscous dissipation and MHD hybrid nanofluid flow towards an exponentially stretching/shrinking surface. Neural Comput Appl. 2021;33:1–11.
[20] Ouyang Y, Md Basir MF, Naganthran K, Pop I. Unsteady magnetohydrodynamic tri-hybrid nanofluid flow past a moving wedge with viscous dissipation and Joule heating. Phys Fluids. 2024;36(6):062009.
[21] Merkin J. On dual solutions occurring in mixed convection in a porous medium. J Eng Math. 1986;20(2):171–9.
[22] Merkin J. Mixed convection boundary layer flow on a vertical surface in a saturated porous medium. J Eng Math. 1980;14(4):301–13.
[23] Bachok N, Ishak A, Pop I. Boundary-layer flow of nanofluids over a moving surface in a flowing fluid. Int J Therm Sci. 2010;49(9):1663–8.
[24] Harris S, Ingham D, Pop I. Mixed convection boundary-layer flow near the stagnation point on a vertical surface in a porous medium: Brinkman model with slip. Transport Porous Media. 2009;77:267–85.
[25] Roşca AV, Pop I. Flow and heat transfer over a vertical permeable stretching/shrinking sheet with a second order slip. Int J Heat Mass Transfer. 2013;60:355–64.
[26] Roşca AV, Pop I. Flow and heat transfer of Powell-Eyring fluid over a shrinking surface in a parallel free stream. Int J Heat Mass Transfer. 2014;71:321–7.
[27] Najib N, Bachok N, Arifin NM. Stability of dual solutions in boundary layer flow and heat transfer over an exponentially shrinking cylinder. Indian J Sci Tech. 2016;9:1–6.
[28] Yasin MHM, Ishak A, Pop I. Boundary layer flow and heat transfer past a permeable shrinking surface embedded in a porous medium with a second-order slip: A stability analysis. Appl Therm Eng. 2017;115:1407–11.
[29] Devi SU, Devi SA. Heat transfer enhancement of Cu–Al_2O_3/water hybrid nanofluid flow over a stretching sheet. J Nigerian Math Soc. 2017;36(2):419–33.
[30] White FM, Majdalani J. Viscous fluid flow. vol. 3. New York: McGraw-Hill; 2006.
[31] Adnan, Ashraf W. Thermal efficiency in hybrid (Al_2O_3–CuO/H_2O and ternary hybrid nanofluids (Al_2O_3–CuO/H_2O) by considering the novel effects of imposed magnetic field and convective heat condition. Waves Random Complex Media. 2022;32:1–16.
[32] Wang C. Stagnation flow towards a shrinking sheet. Int J Non-Linear Mech. 2008;43(5):377–82.
[33] Naganthran K, Nazar R, Pop I. Unsteady stagnation-point flow and heat transfer of a special third grade fluid past a permeable stretching/shrinking sheet. Scientif Reports. 2016;6(1):24632.
[34] Myers TG, Ribera H, Cregan V. Does mathematics contribute to the nanofluid debate? Int J Heat Mass Transfer. 2017;111:279–88.
[35] Ouyang Y, Basir MFM, Naganthran K, Pop I. Dual solutions in Maxwell ternary nanofluid flow with viscous dissipation and velocity slip past a stretching/shrinking sheet. Alexandr Eng J. 2024;105:437–48.
[36] Ouyang Y, Basir MFM, Naganthran K, Pop I. Triple solutions for unsteady stagnation flow of tri-hybrid nanofluid with heat generation/absorption in a porous medium. Case Stud Therm Eng. 2024;61:105027.
[37] Naganthran K, Nazar R. Unsteady boundary layer flow of a Casson fluid past a permeable stretching/shrinking sheet: paired solutions and stability analysis. In: Journal of Physics: Conference Series. vol. 1212. IOP Publishing; 2019. p. 012028.
[38] Basir MFM, Hafidzuddin MEH, Naganthran K, Chaharborj SS, Kasihmuddin MSM, Nazar R, et al. Stability analysis of unsteady stagnation-point gyrotactic bioconvection flow and heat transfer towards the moving sheet in a nanofluid. Chin J Phys. 2020;65:538–53.
[39] Hanif H, Khan A, Rijal Illias M, Shafie S. Significance of Cu-Fe_3O_4 on fractional Maxwell fluid flow over a cone with Newtonian heating. J Taibah Univ Sci. 2024;18(1):2285491.
[40] Saleem S, Animasaun I, Yook SJ, Al-Mdallal QM, Shah NA, Faisal M. Insight into the motion of water conveying three kinds of nanoparticles shapes on a horizontal surface: significance of thermo-migration and Brownian motion. Surfaces Interfaces. 2022;30:101854.